JOURNAL OF MATERIALS SCIENCE **37** (2002) 3229–3239

Effects of grinding process on residual stresses in nanostructured ceramic coatings

XIANBING LIU, BI ZHANG*
The Department of Mechanical Engineering, University of Connecticut, Storrs, CT 06269, USA
E-mail: zhang@engr.uconn.edu

This paper investigates the depth profiles of residual stresses using the $\sin^2\psi$ method combined with grazing incident X-ray diffraction (GIXD) technique. It specifically focuses on the effects of grinding process on the residual stresses in the thermally sprayed nanostructured WC/12Co and $Al_2O_3/13TiO_2$ (*n*-WC/12Co and *n*-$Al_2O_3/13TiO_2$) coatings on low carbon steel substrates. The influence of grinding parameters, such as depth of cut (DOC), table feedrate, abrasive grit size and wheel bond type, on residual stresses is studied. The conditions and limitations of X-ray diffractometry for residual stress measurements are discussed. Discussed also is the difference between the average and actual depth profiles of residual stresses. The paper introduces a method for retrieving the actual depth profiles from the measured average depth profiles. Finally, the influence of peak broadening of grain size, anisotropy from different diffraction planes and surface finish of the samples on the measurement results is explored.

1. Introduction

Thermal spray is a technique of applying metallic or ceramic surface coatings to other base materials, which basically includes two varieties: plasma and flame spraying. The mechanical properties and structure of the coatings formed by plasma and flame spray are the topics of many researches [e.g., 1, 2], and depend on a number of factors, such as the powder grain properties, the substrate material properties and the thermal spray conditions. One of the methods to improve thermal spray quality is to decrease the powder grain size. Materials with fine-scale microstructures have been recognized to exhibit technologically attractive properties. When the grain size of a material decreases to the nanometer scale (tens of nanometers), one obtains a novel class of materials, called "nanostructured materials", which possesses properties different from those conventional materials [3, 4]. Nanostructured tungsten carbide/cobalt (*n*-WC/12Co) and nanostructured alumina/titania (*n*-$Al_2O_3/13TiO_2$) coatings are used in the current study.

In many applications, good surface finish and precise dimensions are needed for coated components. Grinding is a widely used method in machining hard and brittle materials such as ceramics and their coatings. In this study, superabrasive grinding is employed to machine *n*-WC/12Co and *n*-$Al_2O_3/13TiO_2$ coatings. The grinding process can produce residual stresses in a stress-free sample or alter the existing residual stress state of a sample.

On the other hand, the coated components are commonly accompanied with residual stresses caused by the thermal spraying process [5–7]. The residual stresses can result in spallation and cracking of the coatings. Residual stresses due to grinding can alter the residual strength [8] as well as the wear resistance of the ground workpieces [9, 10].

The methods for residual stress measurement in the coatings usually include material removal method, substrate curvature method and diffraction method. In the material removal method, strain gauges are attached to the coating or the substrate to measure the strain changes during drilling a hole in a coated sample [11] or removing a layer of the coating [12, 13]. This method is destructive and can easily result in inaccuracies during material removal. The substrate curvature method is realized by measuring the changes of the substrate curvature caused by the residual stresses in the coating [14]. This method is simple, but is limited by sample shape and dimensions.

The X-ray diffraction method is the most popular one for direct measurement of residual stresses, which is based on the lattice space change. That is reflected by the peak position change in the X-ray intensity pattern. The residual stresses in the coatings result in the lattice space change [6, 7, 15–17]. This method is non-destructive and flexible on the requirements of sample dimensions. Due to the limitations of X-ray penetration depth, the X-ray diffraction method can only be used for surface layer usually of tens of micrometers in

*Author to whom all correspondence should be addressed.

thickness. Neutron diffraction is another choice for measuring the residual stresses [18], which can overcome the small penetration depth limitation of the X-ray diffraction method. However, the neutron diffraction has its own shortcomings such as low scattering intensity and limited availability of the neutron.

The current study is aimed at measuring the residual stresses induced by thermal spraying process, and more importantly at investigating the effects of grinding process on the residual stresses in the thermally sprayed n-WC/12Co and n-Al_2O_3/13TiO_2 coatings with the X-ray diffraction method. In the meantime, the experimental conditions are presented in detail and the factors that influence the measurement results are discussed.

2. Sample preparation and characterization

Nanoscale powders present difficulties for thermal spraying process due to their high specific surface energies and inability to be carried in a moving gas stream and deposited on a substrate. In order to successfully apply nanoscale powders to thermal spraying process, a reconstitution process has been developed [19, 20]. In the reconstitution process, the nanoscale powders are dispersed into colloidal suspension and then a binder is added. Through the subsequent spray, the nanoscale powders are dried into sprayable spherical microscale granules. This method has successfully been used to make sprayable granules from metallic, ceramic and composite nanoscale powders.

In this study, low carbon steel substrates with dimensions of $25 \times 75 \times 4$ mm^3 were used for spray coatings of nanostructured materials. The substrates were then coated with the reconstituted n-WC/12Co granules using the high velocity oxygen fuel (HVOF) method and with n-Al_2O_3/13TiO_2 using the plasma spray. Both coatings had a thickness of around 0.5 mm. The sprayed samples were cut into dimensions of $25 \times 4 \times 4$ mm^3 for grinding experiments and X-ray diffraction measurements. Typical physical properties of n-WC/12Co and n-Al_2O_3/13TiO_2 coatings and low carbon steel substrates are shown in Table I.

The scanning electronic microscope (SEM) photo shows that the n-WC/12Co coating exhibits a large quantity of porosities, but without obvious cracks. The typical surface features of a thermally sprayed n-Al_2O_3/13TiO_2 coating have pores, cracks, microcracks and segmented structures formed by the interconnecting microcracks perpendicular to the coating surface.

TABLE I Typical properties of n-WC/12Co, n-Al_2O_3/13TiO_2 coatings and low carbon steel substrate

Parameters	WC/12Co	Al_2O_3/13TiO_2	Low carbon steel
Powder grain size (nm)	30–50	20–80	–
Mass density (g/cm^3)	14.50	3.9	7.85
Thermal expansion (/K)	6×10^{-6}	5.5×10^{-6}	11.5×10^{-6}
Young's modulus (GPa)	222	70	202
Poisson's ratio	0.22	0.25	0.30
Mass absorption coeff.	184.023	44.183	–

3. Grinding experiment

Grinding experiments were conducted on a precision ceramic grinding machine (Dover Model 956-S) with the computer numerical control (CNC). The machine had aerostatic bearings for its spindle and x, y, z slideways. The spindle had an axial run-out of 0.05 μm and the three slideways had a straightness error of 0.1 μm/25 mm. A laser interferometer was equipped to the machine that formed feedback loops for the x, y, z slideways with a resolution of 0.07 μm. The loop stiffness of the machine was measured to be 50 N/μm. Cup-type diamond grinding wheels were used to grind the coated samples. The grinding wheels had three different bond types and also three grit sizes for the purpose of investigating the effects of bond type and grit size on grinding-induced residual stresses.

The wheel speed was set to 33 m/s or 3500 rpm. In order to investigate the effect of material removal rate (MRR) on residual stresses, depths of cut were set to 2, 5, 15 and 30 μm and feedrates were at 1, 4, and 8 mm/s for the grinding experiments.

4. Residual stress measurement method and GIXD technique

The widely accepted $\sin^2\psi$ technique was used for residual stress characterization in this study. The direction of the measured strain $\varepsilon_{\phi\psi}$ is defined by the azimuth angle ϕ and the tilt angle ψ. The position shift of the peaks in the X-ray diffraction pattern reflects the lattice plane spacing change, and therefore the residual stress. The lattice plane spacing follows Bragg's law,

$$\lambda = 2d_{hkl} \sin\theta \tag{1}$$

where λ is the radiation wavelength, d_{hkl} (hkl are the Miller's indices of the diffraction plane.) is the lattice plane spacing, and θ is the diffraction angle.

Therefore, the measured strain $\varepsilon_{\phi\psi}$ along the (ϕ, ψ) direction is

$$\begin{aligned}\varepsilon_{\phi\psi} &= \frac{d_{\phi\psi} - d_0}{d_0} = \frac{\sin\theta_0}{\sin\theta} - 1 \\ &= \left(\varepsilon_{11}\cos^2\phi + \varepsilon_{12}\sin 2\phi + \varepsilon_{22}\sin^2\phi\right)\sin^2\psi \\ &\quad + \left(\varepsilon_{13}\cos\phi + \varepsilon_{23}\sin\phi\right)\sin 2\psi + \varepsilon_{33}\cos^2\psi\end{aligned} \tag{2}$$

where d_0 is the unstressed lattice plane spacing, $d_{\phi\psi}$ the stressed lattice plane spacing, and θ_0 and θ the diffraction angles corresponding to the unstressed and stressed states, respectively.

According to Hooke's law, using index notation, the relationship between strain and stress is as follows,

$$\varepsilon_{ij} = \frac{1+\nu}{E}\sigma_{ij} - \delta_{ij}\frac{\nu}{E}\sigma_{kk} \tag{3}$$

where i, j and $k = 1, 2, 3$, E and ν are Young's modulus and Poisson's ratio of the coating, respectively.

After Equation 3 being substituted into Equation 2, the following equation of residual stresses can be

obtained,

$$\varepsilon_{\phi\psi}(\tau) = \frac{1+\nu}{E}\left(\sigma_{11}\cos^2\phi + \sigma_{12}\sin 2\phi + \sigma_{22}\sin^2\phi - \sigma_{33}\right)\sin^2\psi + \frac{1+\nu}{E}\sigma_{33} + \frac{1+\nu}{E}(\sigma_{13}\cos\phi + \sigma_{23}\sin\phi)\sin 2\psi - \frac{\nu}{E}(\sigma_{11}+\sigma_{22}+\sigma_{33}) \quad (4)$$

With the assumption of biaxial stress, that is, σ_{13}, σ_{23} and $\sigma_{33} = 0$, the above equation can be simplified as

$$\varepsilon_{\phi\psi}(\tau) = \frac{1+\nu}{E}\left(\sigma_{11}\cos^2\phi + \sigma_{12}\sin 2\phi + \sigma_{22}\sin^2\phi\right) \times \sin^2\psi - \frac{\nu}{E}(\sigma_{11}+\sigma_{22}) = \frac{\sin\theta_0}{\sin\theta} - 1 \quad (5)$$

With the above $\sin^2\psi$ method, the residual stress distributions can be determined from X-ray wavelengths for different depths [21, 22]. Because different wavelength can be obtained by changing the radiation sources, which is sometimes troublesome, a combination of the $\sin^2\psi$ method and the layer removal process can enable a series of stress measurements in depth direction [22]. However, this method is destructive and the removal process can easily alter the stress state in the samples.

The penetration of an X-ray beam is basically dependent on the diffraction plane and the incident angle α used in the measurement. The GIXD technique, which is enabled by the parallel optics of the X-ray diffractometer, is to change the incident angle to obtain different penetration depths. This technique was used in this study to obtain the stress depth profiles. The effective X-ray penetration depth, τ, under an incident angle, α, is as follows [23],

$$\tau = \frac{1}{\rho(\mu/\rho)(1/\sin\alpha + 1/\sin\beta)} \quad (6)$$

where $\beta = 2\theta - \alpha$; ρ is the mass density of the sample; μ is the linear absorption coefficient of the sample for X-ray.

Before calculating the penetration depth τ of X-ray in a material, the mass absorption coefficient, μ/ρ, should be found first. The mass absorption coefficient, μ/ρ, of a material containing more than one element can be calculated from the following expression [22],

$$\frac{\mu}{\rho} = w_1\left(\frac{\mu}{\rho}\right)_1 + w_2\left(\frac{\mu}{\rho}\right)_2 + \cdots \quad (7)$$

where w_1, w_2, etc, are the weight fractions of elements in the material and $(\frac{\mu}{\rho})_1$, $(\frac{\mu}{\rho})_2$, etc., are the elements' mass absorption coefficients with respect to the given radiation wavelength. The mass absorption coefficients for n-WC/12Co and n-Al_2O_3/13TiO_2 with respect to Cu-K_α are calculated based on Equation 7 and listed in Table I. Table II lists the effective penetration depths for Cu-K_α radiation in n-WC/12Co and n-Al_2O_3/13TiO_2 coatings.

TABLE II Effective penetration depths for Cu-K_α radiation in n-WC/12Co and n-Al_2O_3/13TiO_2 coatings

Angles of incidence α (°)	Effective penetration depth in n-WC/12Co, τ (μm)	Effective penetration depth in n-Al_2O_3/13TiO_2, τ (μm)
3	0.1827	2.8695
5	0.2898	4.6017
10	0.5083	8.3409
15	0.6590	11.2880
20	0.7443	13.4899
25	0.7652	14.9769
30	–	15.7678

5. Measurement results and discussions

5.1. Residual stresses in as-sprayed coatings

In thermally sprayed coatings, the residual stresses mainly originate from the combined effect of the splat quenching and the mismatch in thermal expansion between the coating and substrate. When high-temperature particles hit the substrate, the particles quickly quench due to a large difference in temperature. During the quenching process, the contraction of the deposited coating is constrained by the substrate due to adhesion. The tensile quench stress is created in the coating. In the meantime, the substrate temperature also increases. After deposition, the coating and substrate cool down to the room temperature. During the cooling process, the mismatch stress develops due to the difference between the two thermal expansion coefficients of the coating and substrate. The mismatch stress could be tensile or compressive and is determined by the difference of the two thermal expansion coefficients. For the coatings used in this paper, the thermal expansion coefficient of substrate material (low carbon steel) is close to twice of that of n-WC/12Co and over twice of that of n-Al_2O_3/13TiO_2 (Table I), both of which result in compressive mismatch stress.

The final residual stresses in the coatings are determined by the combined effect of quenching stress and thermal mismatch stress. Biaxial stresses can form under the conditions that the substrate is flat, smooth and large enough in width and length, and the thickness of the substrate is much larger than that of the coating. With the GIXD technique, the assumption that there is no significant stress gradient in the thickness direction becomes unnecessary.

The measurement was carried out on an X-ray diffractometer (Bruker AXS), equipped with parallel beam optics. The measurement conditions and configuration are listed in Table III. In the following depth profile measurements, the incident angles of 3–25° were used for the n-WC/12Co coatings and 3–30° for the n-Al_2O_3/13TiO_2 coatings. For other measurements, the incident angle of 25° (penetration depth of 0.7652 μm) was fixed for the n-WC/12Co coatings and 30° (the

TABLE III Measurement conditions and configuration

Diffractometer	
Optics	Parallel beam geometry with Glober Mirror
X-ray radiation source	Cu-K_α
Radiation wavelength, λ	0.15406 nm
Incident slit	1.5°
Detector slit	2.0°
Detector	Scintillation counter
Step size	0.02°
Scanning speed	0.5°/min
Incident angles	3.0°–30°
Nanostructured coatings	
Materials	n-WC/12Co and n-Al_2O_3/13TiO_2
Diffraction lattice	Hexagonal (WC) and Rhombohedral (Al_2O_3)
Diffraction plane (hkl)	WC (100), WC (101), Al_2O_3 (214)
Diffraction angles ($2\theta_0$)	WC: 35.627° (100), 48.627° (101) Al_2O_3: 66.516 (214)
Measurement directions (ϕ)	0°, 90°

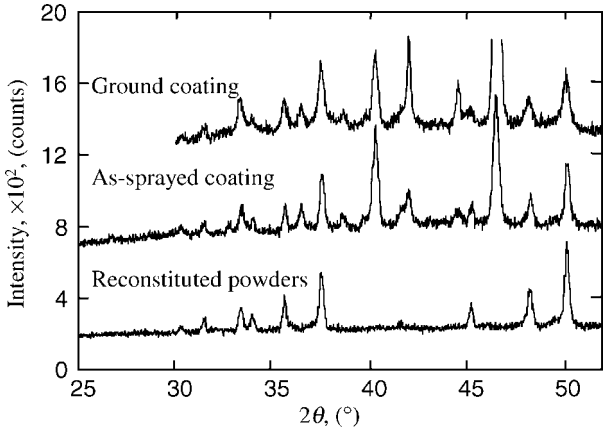

Figure 1 X-ray diffraction patterns of reconstituted powders, as-sprayed coating and ground coating of n-WC/12Co.

penetration depth of 15.7678 μm) for the n-Al_2O_3/13TiO_2 coatings. Except particular specification, the diffraction planes used were WC(101) and Al_2O_3(214).

Fig. 1 shows the X-ray diffraction patterns of the reconstituted powder, the as-sprayed coating and the ground coating of n-WC/12Co. Comparing the three patterns, the change of the diffraction intensity and the 2θ position of the peaks can be observed, which means that the thermal spray and grinding process are accompanied by a texture change in the coating and hence result in residual stresses.

Equation 5 is used to calculate the residual stresses (σ_{xx} and σ_{yy}) in the current two as-sprayed and ground coatings. The depth profiles of residual stresses are shown in Fig. 2 for as-sprayed n-WC/12Co coatings and Fig. 3 for as-sprayed n-Al_2O_3/13TiO_2 coatings. Fig. 2 shows that the residual stresses σ_{xx} and σ_{yy} in the as-sprayed n-WC/12Co coatings are tensile and both of their values are close to 150 MPa. This means that there exits no anisotropy in the plane parallel to the substrate surface in the current as-sprayed n-WC/12Co coatings for residual stresses. The depth profile indicates that there is no significant gradient in the thickness direction, which agrees to the assumption used in some references [e.g., 6, 17].

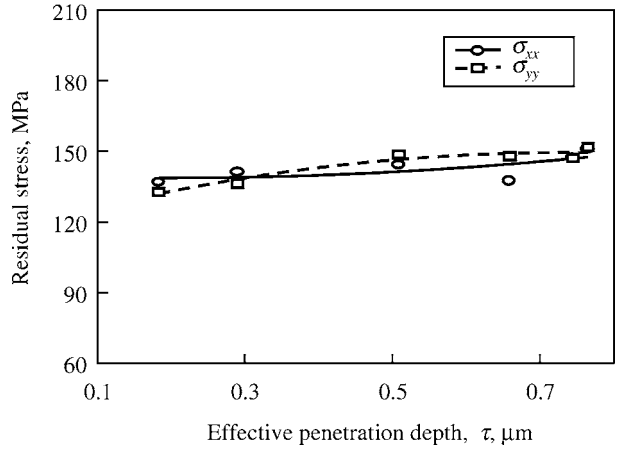

Figure 2 Depth profiles of residual stresses in the as-sprayed n-WC/12Co coatings.

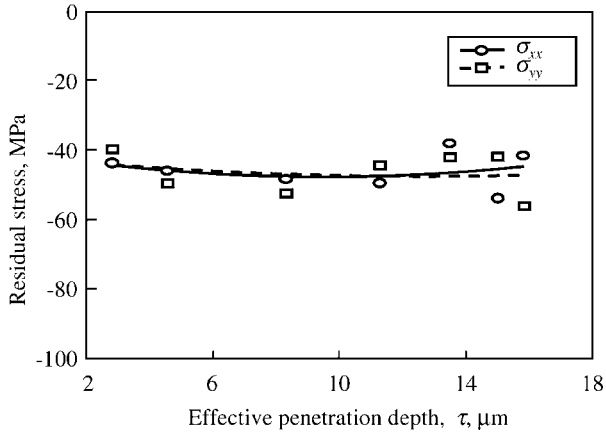

Figure 3 Depth profiles of residual stresses in the as-sprayed n-Al_2O_3/13TiO_2 coatings.

As shown in Fig. 3, compressive residual stresses σ_{xx} and σ_{yy} exist in the as-sprayed n-Al_2O_3/13TiO_2 coatings and their values reach −45 MPa. Similarly, there is no anisotropy in the plane parallel to the substrate surface and no significant gradient in the thickness direction. The compressive residual stresses mean that the mismatch stress plays a dominant role in the final formation of the residual stresses in the as-sprayed n-Al_2O_3/13TiO_2 coatings. On the contrary, the dominant quenching stress in the thermal spray process determines the tensile residual stress in the as-sprayed n-WC/12Co coatings. A large number of microcracks function as stress relief mechanisms, which limit the magnitude of the residual stresses to a relatively small level for the n-Al_2O_3/13TiO_2 coatings.

5.2. Effects of grinding process on residual stresses

The previous studies [21, 24–26] show that the residual stresses induced in a grinding process appear to be biaxial with stress components $\sigma_\perp(\sigma_{xx})$ perpendicular to and $\sigma_{//}(\sigma_{yy})$ parallel to the grinding direction. Therefore, only two X-ray measurements are required for determining grinding residual stresses in each incident angle. This study performed X-ray measurements in the directions perpendicular to and parallel to the grinding

direction, that is, $\phi = 0^\circ$ and $\phi = 90^\circ$. The measurement conditions and the configuration of X-ray diffraction are the same as in Table III.

5.2.1. Depth profiles of residual stresses

Fig. 4a presents the depth profiles of the residual stresses $\sigma_\perp(\sigma_{xx})$ and $\sigma_{//}(\sigma_{yy})$ in the ground n-WC/12Co coatings. The residual stresses in the near surface layer were found compressive as opposite to those in the as-sprayed coatings. In the near surface layer, $\sigma_\perp(\sigma_{xx})$ is 598 MPa, much larger than $\sigma_{//}(\sigma_{yy})$ of 387 MPa, which means a significant dependence on grinding direction. The directional dependence can be considered to be due to the cutting action of abrasive grits. The portion of material perpendicular to the cutting direction is deformed more plastically than that parallel to the cutting direction by plowing. The compressive stresses and the apparent plastic deformation observed in an SEM image (Fig. 4b) of the ground n-WC/12Co coating surface suggest that the mechanical loading be the main reason for the change of residual stresses in the coatings. If the resultant residual stresses are the superposition of the existing stresses in the as-sprayed coating and those due to grinding, the change in $\sigma_\perp(\sigma_{xx})$ in the near surface layer reaches 750 MPa. Fig. 4a also indicates that a strong gradient exists in the thickness direction in the ground coating.

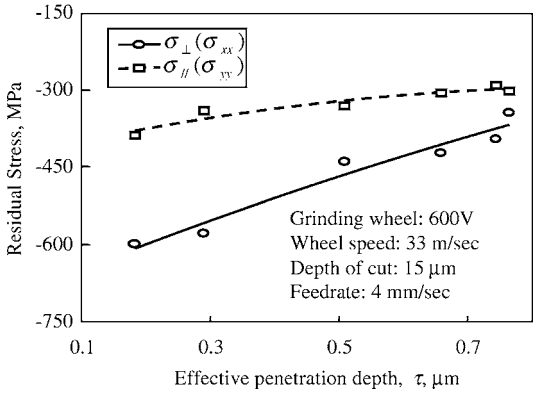

(a)

(b)

Figure 4 Depth profiles of residual stresses and SEM surface image of a ground n-WC/12Co coating. (a) Depth profiles of residual stresses in a ground n-WC/12Co coating, (b) SEM image of the surface of a ground n-WC/12Co coating (grinding conditions shown in (a)).

Under the same grinding conditions, Fig. 5a shows the similar characteristics in the ground n-Al_2O_3/$13TiO_2$ coatings: compressive residual stresses, strong dependence on the grinding direction, and significant gradient in the thickness direction. There were no obvious grinding marks in the ground n-Al_2O_3/$13TiO_2$ coatings, which are evidenced by the SEM image (Fig. 5b).

5.2.2. Effects of material removal rate

Altering the depth of cut or the feedrate or both changes material removal rate (MRR). For example, MRR can be doubled through doubling the depth of cut or the feedrate. However, the effect of varying the depth of cut or feedrate on the residual stresses induced by the grinding process is different. Figs 6 and 7 show that the residual stress ($\sigma_\perp$) increases with the increase of the depth of cut or feedrate for the ground n-WC/12Co coatings. If comparing Fig. 6 to Fig. 7, one can find that the depth of cut has more influence on the residual stress ($\sigma_\perp$) than the feedrate does. In the current cup-type grinding, the increase of the wheel depth of cut directly results in the growth of the grit depth of cut in the thickness direction while the feedrate change mainly affects the grit cutting in the longitudinal (horizontal) direction and has a relatively small influence on the grit depth of cut.

Fig. 8a shows the change of the residual stress ($\sigma_\perp$) with the increase of the depth of cut for the ground n-Al_2O_3/$13TiO_2$ coating. Fig. 8b is the SEM images of the surface of a ground n-Al_2O_3/$13TiO_2$ coating at a depth of cut of 30 μm. Compared to Fig. 5b (where other grinding conditions are the same except that the depth of cut is 15 μm), the apparent grinding marks in Fig. 8b indicates the significant influence of increasing depth of cut. Also the grinding marks suggest that although it is not as obvious as in the ground n-WC/12Co coating, there still exists plastic deformation in the ground n-Al_2O_3/$13TiO_2$ coating when under a large depth of cut. In Fig. 9, it is shown that the residual stress ($\sigma_\perp$) in the ground n-Al_2O_3/$13TiO_2$ coatings also increases with the increase of the feedrate. The similar effects of MRR can be observed on $\sigma_{//}$. In the following parts, only $\sigma_\perp$ will be discussed and the conclusions are applicable to $\sigma_{//}$.

5.2.3. Effect of wheel bond type

Three different bonds, but the same mean grit size of 15 μm, were used for the grinding wheels: vitrified bond, cast iron fiber bond and resin bond. Fig. 10 shows that for the n-WC/12Co coatings, the vitrified bond wheel caused the largest change in the residual stress while the resin bond wheel the smallest. The lower concentration of abrasive grits in the resin bond may partially contribute to this difference, but is considered insignificant. For the n-Al_2O_3/$13TiO_2$ coatings, the bond type effect was less significant, as shown in Fig. 11.

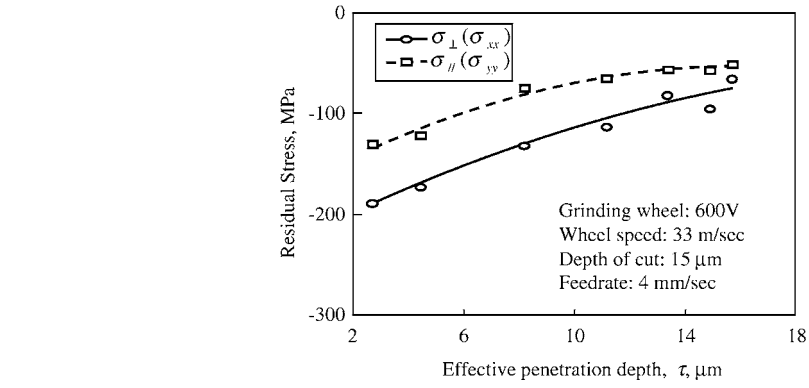

(a)

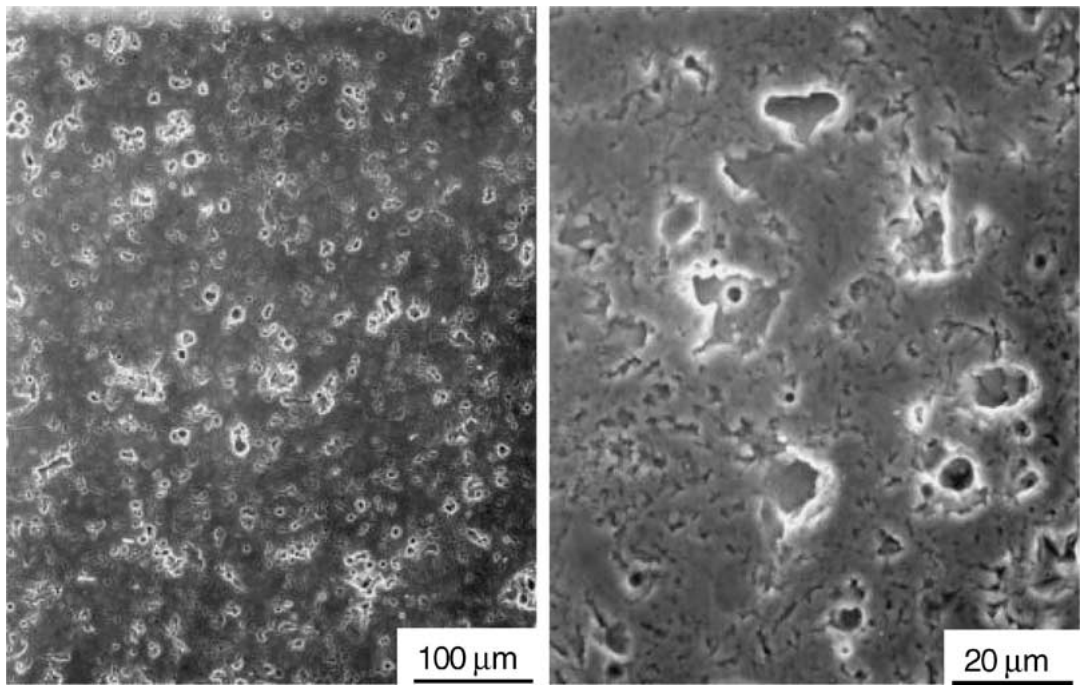

(b)

Figure 5 Depth profiles of residual stresses and SEM surface images of a ground n-Al_2O_3/13TiO_2 coating. (a) Depth profiles of residual stresses in a ground n-Al_2O_3/13TiO_2 coating, (b) SEM observations of a ground n-Al_2O_3/13TiO_2 coating (Grinding conditions shown in (a)).

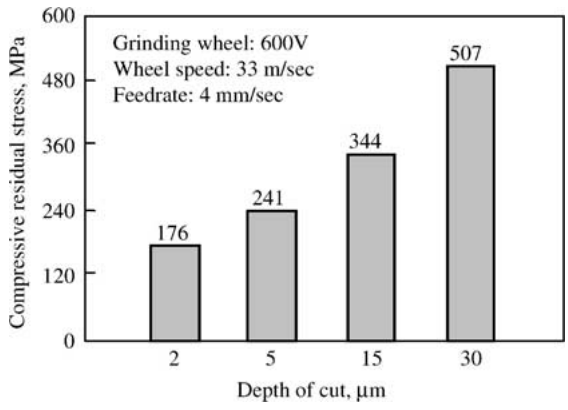

Figure 6 Compressive residual stress $\sigma_{\perp}(\sigma_{xx})$ vs. depth of cut in ground n-WC/12Co coatings.

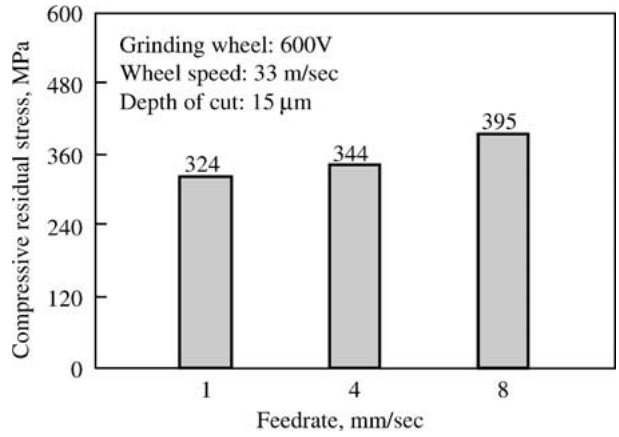

Figure 7 Compressive residual stress $\sigma_{\perp}(\sigma_{xx})$ vs. feedrate in ground n-WC/12Co coatings.

5.2.4. Effect of abrasive grit size

For the n-WC/12Co coatings, the larger the abrasive grit size, the more the influence on the residual stresses. In Fig. 12a, the magnitude of the compressive residual stresses reaches as high as 480 MPa in the n-WC/12Co coatings ground with the 120 V wheel. The 120 V wheel resulted in more ductile deformation as shown in the SEM observation of Fig. 12b compared to Fig. 4b ground by 600 V under the same grinding conditions.

Fig. 13a presents the influence of abrasive grit size on the residual stress in the ground n-Al_2O_3/13TiO_2

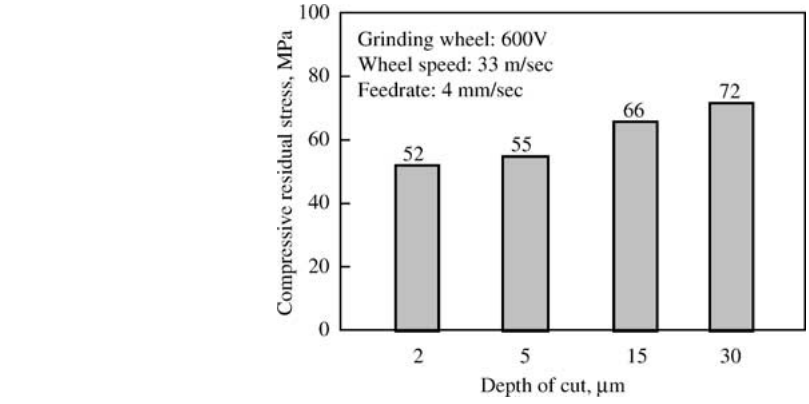

(a)

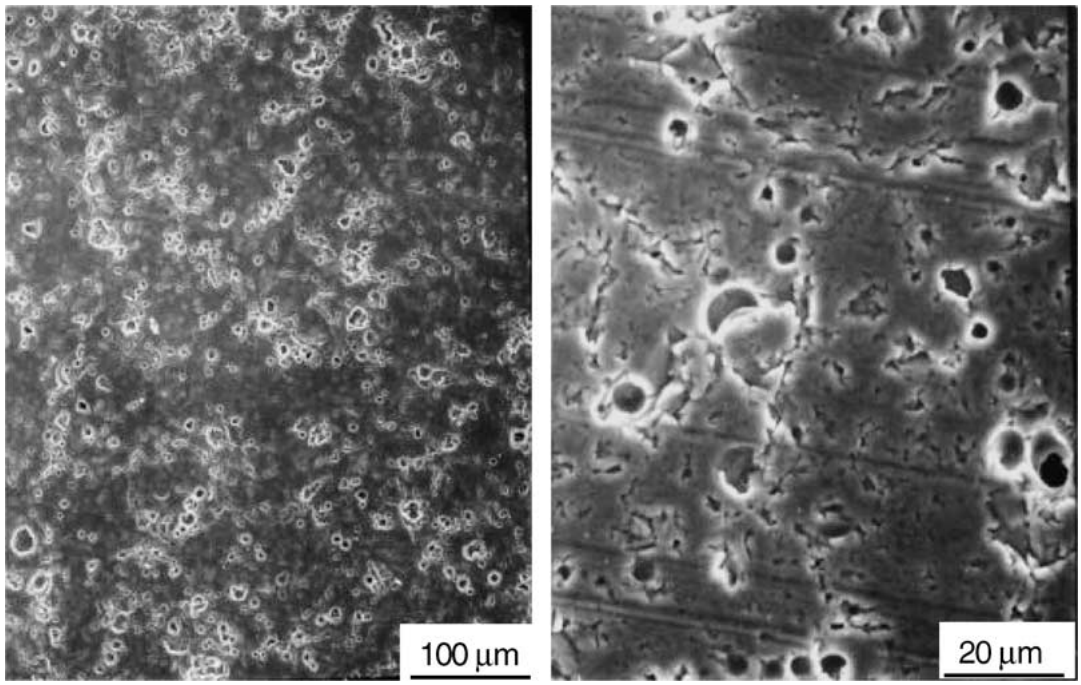

(b)

Figure 8 Effects of depth of cut on residual stress and SEM observations of a ground n-Al_2O_3/13TiO_2 coating at depth of cut = 30 μm. (a) Compressive residual stresses $\sigma_\perp(\sigma_{xx})$ vs. depth of cut in ground n-Al_2O_3/13TiO_2 coating, (b) SEM observations of a ground n-Al_2O_3/13TiO_2 coating at depth of cut = 30 μm (other grinding conditions shown in (a)).

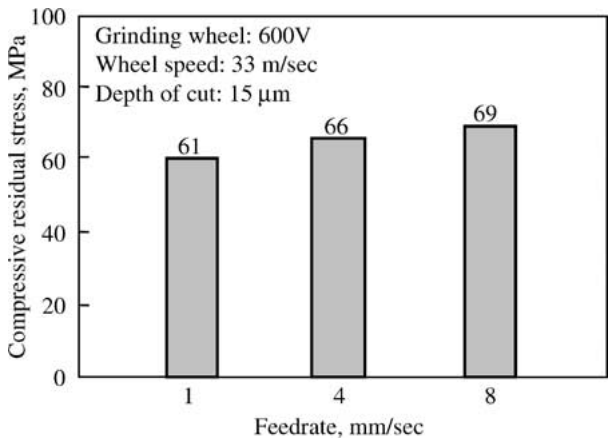

Figure 9 Compressive residual stress $\sigma_\perp(\sigma_{xx})$ vs. feedrate in ground n-Al_2O_3/13TiO_2 coatings.

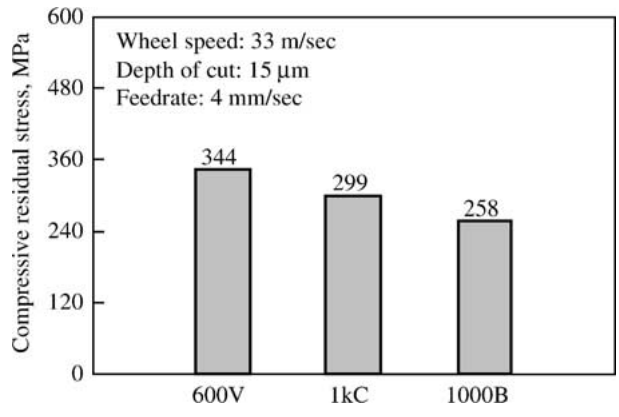

Figure 10 Compressive residual stress $\sigma_\perp(\sigma_{xx})$ vs. different wheel bond types in ground n-WC/12Co coatings.

coatings. First, the grit size effect was not found significant for the ground n-Al_2O_3/13TiO_2 coatings. Second, it is interesting to note that the residual stress with the 120 V wheel was smaller than that with the 600 V wheel, which may be attributed to the fact that under the same grinding conditions, the 120 V wheel induced more chippings and microcracks (Fig. 13b) to a ground sample than the wheels with smaller grit sizes. These damages function as stress relievers and hence suppress the growth of residual stresses.

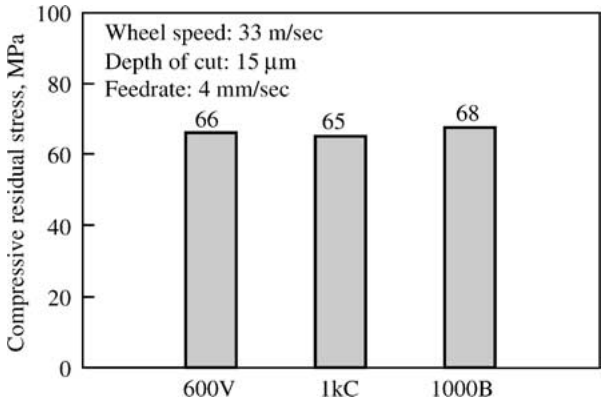

Figure 11 Compressive residual stress $\sigma_{\perp}(\sigma_{xx})$ vs. different wheel bond types in ground n-Al_2O_3/13TiO_2 coating.

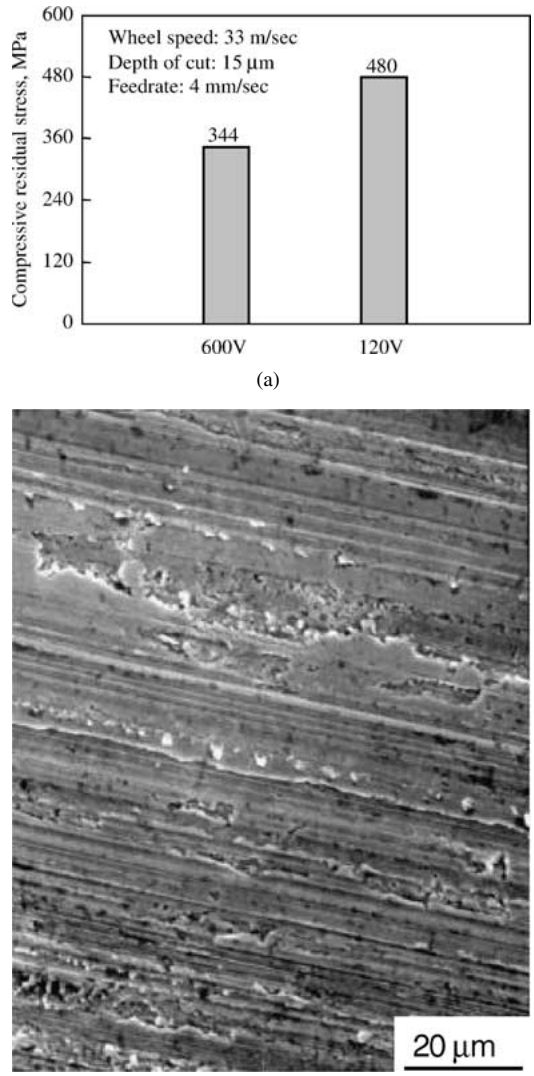

(a)

(b)

Figure 12 Effect of wheel grit sizes on residual stress and SEM observation of an n-WC/12Co coating ground with 120 V wheel. (a) Compressive residual stresses $\sigma_{\perp}(\sigma_{xx})$ vs. wheel grit sizes in a ground n-WC/12Co coating, (b) SEM observation of plastic deformation in an n-WC/12Co coating ground with 120 V wheel (grinding conditions shown in (a)).

5.3. Averaged and actual depth profiles of residual stresses

One should realize that the above residual stresses, determined by the X-ray diffraction method, are averaged over the entire irradiated layer of the sample. The depth profiles, also called τ-profiles, are the depth profiles of average residual stresses. The actual depth profiles of residual stresses, termed z-profiles (where z is the distance from the sample surface) can be retrieved from the measured τ-profiles. τ-profile and z-profile have the following relationship,

$$Q(\tau) = \frac{\int_0^D q(z)e^{-z/\tau}\,\mathrm{d}z}{\int_0^D e^{-z/\tau}\,\mathrm{d}z} \tag{8}$$

where $Q(\tau)$ is the experimentally measured τ-profile; $q(z)$ the corresponding z-profile; D the thickness of a coating.

Equation 8 is a Fredholm integral equation of the first kind. Analytical or numerical method can be used to solve Equation 8 for $q(z)$. The details of analytical method can be found in [27, 28] for a sample with thickness much larger than the maximum X-ray penetration depth. The numerical method is based on the idea that a continuous and bound function can be approximated by piece-wise linear functions. Phillips [29] and Twomey [30] proposed a linear constrained numerical inversion method. Backus-Gilbert method [31] is another inversion numerical method for solving Equation 8 for $q(z)$. Both the methods were designed to control the resolution and stability of the inversion results. The solution of Equation 8 for $q(z)$ is an important topic for X-ray diffraction measurement of residual stresses, which is not discussed in this paper in detail.

Although the profiles of residual stresses presented in this paper are τ-profiles, the obtained information is enough to provide insight into the effect of grinding process on the residual stresses in the ground coatings.

5.4. Peak broadening in X-ray diffraction

For a perfect crystalline material, the diffraction peaks in diffraction pattern should be symmetric and sharp. However, for an actual material, the diffraction peaks are broadened due to crystal defect, micro strain, instrumental effect and small grain size. When the size of crystal grains, such as the nanostructured material powders, is smaller than 0.1 μm, particle size broadening happens, which renders difficulty in the X-ray diffraction measurement. However, prior to thermal spray, the nanostructured powders used in the current study have been reconstituted into micron scale granules. The peak broadening phenomenon was not very obvious in residual stress measurement of the coatings. Fig. 14 shows the diffraction patterns of the reconstituted n-WC/12Co and conventional WC/12Co (Metco) powders. There is no apparent peak broadening phenomenon in the pattern of the reconstituted n-WC/12Co powders.

5.5. Anisotropy

Elastic anisotropy, that is, dependence of elastic constants on (*hkl*) direction in the crystal, was investigated on (331) and (420) in nickel coatings by Matejicek *et al.* [17]. Their research indicates anisotropy in these directions. In this paper, the dependence of effective penetration depth on (*hkl*) direction in the crystal is discussed. Using Equation 6, the effective penetration depths on

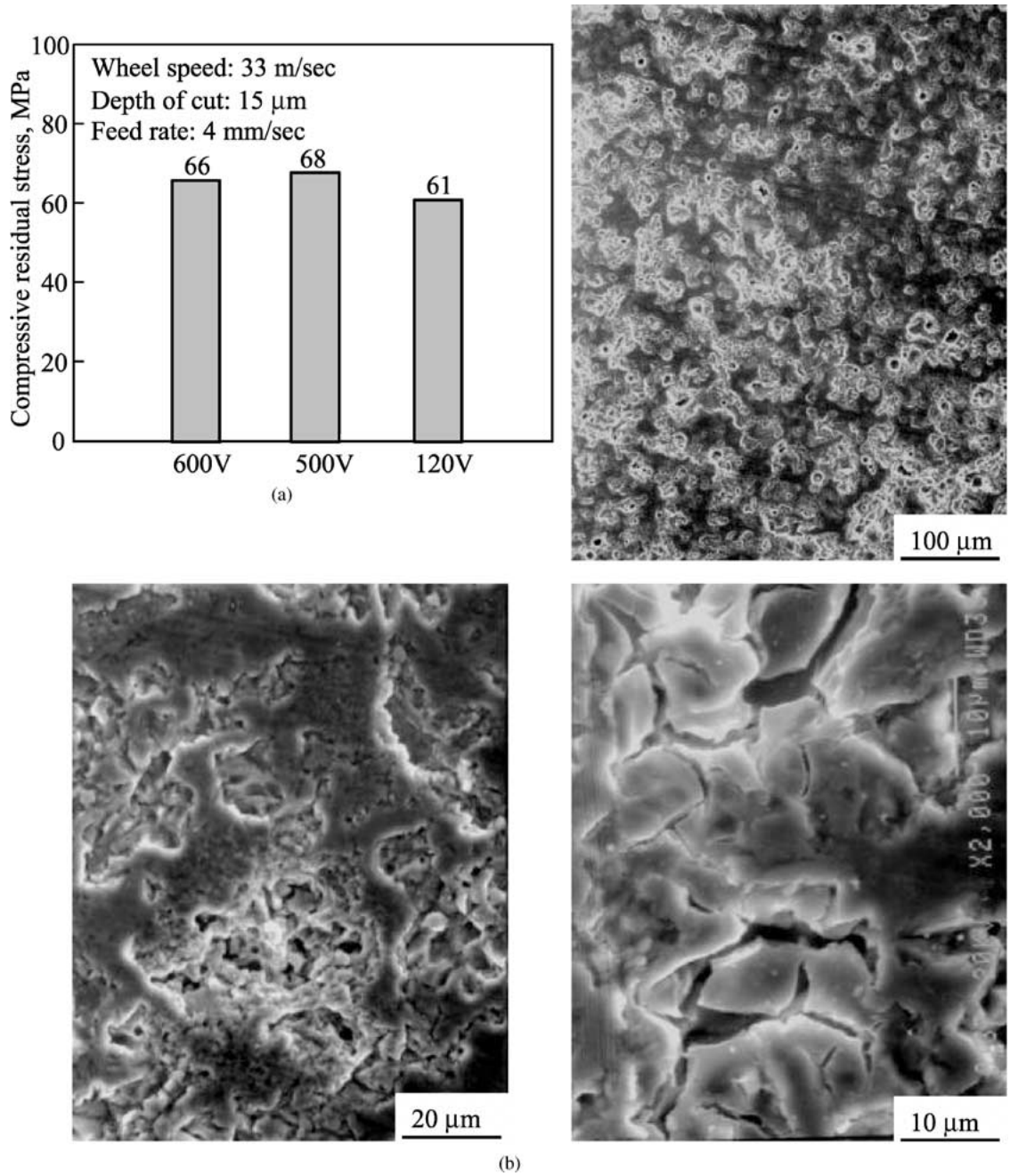

Figure 13 Effect of wheel grit size on residual stress and SEM observations of an n-Al_2O_3/13TiO_2 coating ground with 120 V wheel. (a) Compressive residual stresses $\sigma_{\perp}(\sigma_{xx})$ vs. wheel grit size in ground n-Al_2O_3/13TiO_2 coatings, (b) SEM observations of an n-Al_2O_3/13TiO_2 coating ground with 120 V wheel (grinding conditions shown in (a)).

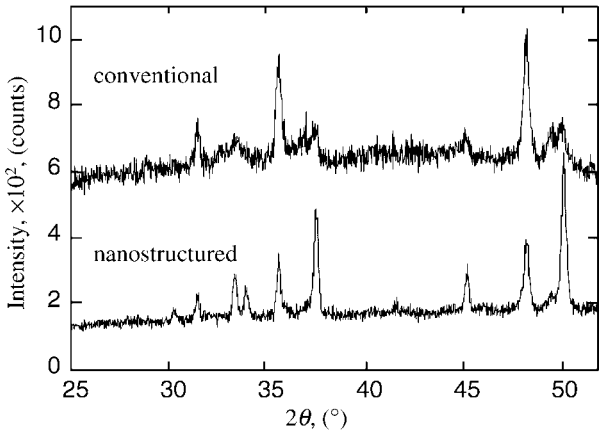

Figure 14 X-ray diffraction patterns of reconstituted n-WC/12Co powders and conventional WC/12Co powders.

diffraction planes WC (100) and WC (101) are listed in Table IV.

From Table IV, one can see that the effective penetration depth first increases with the increase of the incident angle, and then decreases after it reaches a maximum value for each diffraction plane. The anisotropy of the effective penetration depth for different diffraction planes presents in two aspects: first, the effective penetration depths are different for different diffraction planes at the same incident angle; second, the maximum effective penetration depth is reached at different incident angles for different diffraction planes. As discussed above, the average residual stress through the penetration depth is obtained from the X-ray diffraction. Therefore, even with the same other conditions, the measured values of residual stresses will be obtained

TABLE IV Comparison of penetration depths for Cu-Kα_1 on diffraction planes WC (100) and WC (101)

Angles of incidence, α (°)	Effective penetration depth, τ (μm)	
	WC (101)	WC (100)
3	0.1827	0.1788
5	0.2898	0.2789
10	0.5083	0.4643
15	0.6590	0.5592
20	0.7443	0.5647
25	0.7652	0.4812
30	0.7220	0.3072

TABLE V Surface roughness and measured residual stress σ_{xx}

Samples	Surface roughness, Ra (μm)	Measured residual stress, (σ_{xx}) (MPa)
As sprayed	1.25	152
Polished	0.72	155
Polished	0.13	161

differently for different diffraction planes due to their different penetration depths except for the case in which the residual stress is uniform through thickness. It is important to point out the incident angle or effective penetration depth using the X-ray diffraction method when a measurement result is presented, especially in the case with a significant stress gradient existing. In this paper, except for the depth profiles, the residual stresses are presented at an incident angle of 25° or penetration depth of 0.7652 μm for the n-WC/12Co coatings and at an incident angle of 30° or penetration depth of 15.7678 μm for the n-Al_2O_3/13TiO_2 coatings.

5.6. Effect of surface finish

The asperities on the surface of a sample have the stress relaxation effect for the X-ray diffraction measurement results. For the low penetration depth of X-ray ($\sim$0.77 μm in n-WC/12Co and $\sim$16 μm in n-Al_2O_3/13TiO_2), larger surface roughness tends to lower measurement readings for residual stresses. In order to investigate the effect of surface finish on residual stress measurement, the polishing method was used to reduce surface roughness. In the polishing process, a very low load was applied to limit the influence of polishing on the residual stress existing in the coating. Table V lists the surface roughness and the corresponding measured residual stress σ_{xx} of an n-WC/12Co sample.

Table V shows that the residual stress is slightly underestimated for a sample with a rough surface. Surface roughness R_a is usually less than 0.02 μm for the ground n-WC/12Co coatings and less than 0.2 μm for the ground n-Al_2O_3/13TiO_2 coatings. Since the values of the R_a for ground coatings are relatively small compared to the effective penetration depth, the influence of surface roughness on the measurement results can thus be neglected.

6. Conclusions

The X-ray diffraction method is employed to measure the residual stresses in the as-sprayed and ground nanostructured WC/12Co and Al_2O_3/13TiO_2 coatings. The conventional $\sin^2\psi$ method combined with the grazing incident X-ray diffraction technique is applied to obtain the depth profiles of the residual stresses in the as-sprayed and ground samples. The theoretical background and assumptions, which justify the application of the current method, are discussed in detail. The formation of the residual stresses in the as-sprayed coatings is investigated.

The measurement results show that tensile stresses exist in the as-sprayed nanostructured WC/12Co coatings while compressive stresses in the as-sprayed nanostructured Al_2O_3/13TiO_2 coatings. From the depth profiles of the residual stresses, one can see that there is no significant gradient in the thickness direction and the stresses in the plane parallel to the surface of a substrate are isotropic for the two types of as-sprayed coatings.

The depth profiles of the residual stresses in the coatings ground with the 600 V wheel show that the residual stresses have a significant dependence on the grinding direction ($\sigma_\perp > \sigma_{//}$) and a strong gradient in the thickness direction. The mechanical loading (grinding) plays a major role in changing the state of the sample residual stresses.

The residual stresses induced by the grinding process increases with the increase of wheel depth of cut or feedrate or both. For the cup-type wheels, it is found that the wheel depth of cut has more influence than does the feedrate. In addition, the wheel bond type has an obvious effect on the alternation of residual stresses for the nanostructured WC/12Co coatings while almost no effect for the nanostructured Al_2O_3/13TiO_2 coatings. When compared to the 600 V wheel, the larger grit size in the 120 V wheel has more effect on the residual stresses in the ground nanostructured WC/12Co coatings. However, the chippings and microcracks induced by the large grits in the 120 V wheel have a relief effect on the residual stresses in the ground nanostructured Al_2O_3/13TiO_2 coatings and hence lead to a lower level of residual stresses.

The current study is helpful in understanding the residual stress state in coatings and in selecting the grinding parameters to control residual stresses to a desired state.

Acknowledgment

The authors gratefully acknowledge the financial support from Connecticut Innovations, Inc. (CT) and the supply of coating samples from Inframat Corporation. Thanks also go to Mr. Jayant Dey and Mr. Zhaohui Deng for their assistance in the grinding experiment, and S. L. Munson & Company and Tokyo Diamond Tools Mfg. Co. for their donation of some diamond wheels.

References

1. T. HU, L. STEIHL, W. RAFANIELLO, T. FAWCETT, D. D. HAWN, J. G. MASHALL, S. J. ROZEVELD, C. L. PUTZIG, J. H. BLACKSON, W. CERMIGNANI and M. G. ROBINSON, *Thin Solid Films* **332** (1998) 80.
2. N. PARKANSKY, I. I. BEILIS, L. RAPOPORT, R. L. BOXMAN, S. GOLDSMITH and R. YU, *Surface & Coatings Technology* **105** (1998) 130.
3. R. BIRRINGER, *Materials Science and Engineering* A **117** (1989) 33.

4. B. H. KEER and P. R. STRUTT, *Powder and Particle* **13** (1995) 45.
5. Y. D. LEE and F. ERDOGAN, *International Journal of Fracture* **69** (1995) 145.
6. T. W. CLYNE and S. C. GILL, *Journal of Thermal Spray Technology* **5**(4) (1996) 401.
7. I. IORDANOVA and K. S. FORCEY, *Surface and Coatings Technology* **91** (1997) 174.
8. R. W. MONAHAN, B. ZHANG, F. YANG, J. WANG and Z. ZHU, *J. Mat. Sci.* **35** (2000) 1115.
9. H. K. TÖNSHOFF and H. G. WOBKER, *Jour. Lubr. Engr.* **47**(7) (1990) 579.
10. P. ROTH, H. G. WOBKER and C. MENZ, *Tribology Transactions* **35** (1995) 714.
11. V. DOLHOF, J. MUSIL, M. CEPERA and J. ZEMAN, "Thermal Spray Science and Technology," edited by C. C. Berndt and S. Sampath (ASM International, 1995) 445.
12. D. J. GREVING, J. R. SHADLEY and E. F. RYBICKI, *Journal of Thermal Spray Technology* **3**(4) (1994) 371.
13. D. J. GREVING, E. F. RYBICKI and J. R. SHADLEY, "Thermal Spray Industrial Applications," edited by C. C. Berndt and S. Sampath (ASM International, 1994) 647.
14. M. FINOT, S. SURESH, C. BULL and S. SAMPATH, *Materials Science & Engineering* A **205** (1996) 59.
15. M. LEVIT, I. GRIMBERG and B. Z. WEISS, *ibid.* **206** (1996) 30.
16. O. KESLER, J. MATEJICEK, S. SAMPATH, S. SURESH, T. GNAEUPEL-HEROLD, P. C. BRAND and H. J. PRASK, *ibid.* **257** (1998) 215.
17. J. MATEJICEK, S. SAMPATH and J. DUBSKY, *Journal of Thermal Spray Technology* **7**(4) (1998) 489.
18. M. T. HUTCHINGS, "Measurement of Residual and Applied Stress Using Neutron Diffraction," edited by M. T. Hutchings and P. J. Withers (Kluwer Academic Publishers, 1992) p. 3.
19. P. R. STRUTT, R. F. BOLAND and B. H. KEAR, US patent filed, November 1995.
20. T. D. XIAO, S. JIANG, M. D. WANG, Y. WANG, R. ZATORSKI, C. W. STROCK and P. R. STRUTT, 12th Intl. Surface Modification Conference, ASM Intl., 1998.
21. P. ROTH, H. G. WOBKER and C. MENZ, *Tribology Transactions* **35** (1995) 714.
22. B. D. CULLITY, "Elements of X-ray Diffraction," 2nd edn. (Addison-Wesley Publication Company, 1978).
23. U. WÖLFSTIEG, *Harterei-Tech, Mitt.* **31**(83) (1976).
24. H. K. TÖNSHOFF, H. SIEMER and H-G. WOBKER, Intersociety Symposium on Machining of Advanced Ceramic Materials and Components, Chicago, IL, USA, 1988.
25. S. IMMELMANN, E. WELLE and W. REIMERS, *Materials Science and Engineering* **238** (1997) 287.
26. H. YOSHIDA, Y. NANAYAMA and Y. MORIMOTO, *Advances in X-Ray Analysis* **32** (1989) 443.
27. E. D. ROLL, R. N. PANGBORN and M. F. AMATEAU, "Non-Destructive Characterization of Materials II" (Plenum Press, 1987) p. 595.
28. P. K. PREDECKI, *Powder Diffraction* **8**(2) (1993) 122.
29. D. L. PHILLIPS, *Journal of the Association for Computing Machinery* **9** (1962) 84.
30. S. TWOMEY, *ibid.* **10** (1963) 97.
31. G. E. BACKUS and F. GILBERT, *Geophysical Journal of the Royal Astronomical Society* **13** (1967) 247.

Received 14 June 2001
and accepted 7 February 2002